Hindawi
Advances in Civil Engineering
Volume 2021, Article ID 6653592, 23 pages
https://doi.org/10.1155/2021/6653592

Research Article

Seismic Behavior of Nonductile RC Frame Slotted with Corrugated Steel Plate Shear Walls

Ningning Feng [1,2] **and Changsheng Wu** [1]

[1]*Department of Civil and Architecture Engineering, Changzhou Institute of Technology, Changzhou 213032, China*
[2]*School of Engineering, University of British Columbia, Okanagan, BC, Canada*

Correspondence should be addressed to Ningning Feng; fengningning1104@163.com

Received 22 October 2020; Revised 14 February 2021; Accepted 17 March 2021; Published 30 March 2021

Academic Editor: Hanbing Bian

Two specimens of nonductile reinforced concrete (RC) frame (ND-1) and nonductile RC frame retrofitted by corrugated steel plate shear walls slotted with columns (ND-2) are established by finite element. These specimens have same dimensions and steel skeletons. Finite element models had been verified by the existing experimental results. The hysteresis curves, skeleton curves, ductility, and stiffness curves of Specimen ND-1 and Specimen ND-2 are compared. The results show that the reinforcement effect is significant. Twenty-four models are built to study the seismic behavior on different influence parameters. The parameters are slit width, thickness of corrugated steel plate shear walls, concrete strength of nonductile RC frame, and boundary conditions of corrugated steel plate shear walls at slotted parts. The results indicate that the strength is declined with the increase of slit width. With the increase of thickness and concrete strength, the strength and stiffness are enhanced. The strength is larger with the boundary than without. Slit width and thickness have an important impact on the stiffness. Concrete strength and boundary conditions have little impact on stiffness. The strengthened nonductile RC frames have enough ductility.

1. Introduction

In earthquake zones of China, there were number of older, low-rise concrete buildings which have not been retrofitted for earthquake safety. These two-storey to five-storey structures may meet the old building-code standards. However, new building codes reflected later earthquake engineering research and incorporated structural elements that allowed concrete buildings to bend and stretch a bit during earthquakes. Older designs were short of those details. There were hundreds of thousands of buildings that have not been retrofitted. Those brittle buildings were called "nonductile RC" buildings. "Ductile" meant flexible, while "reinforced concrete" refers to concrete embedded with material such as steel mesh and rebar. From an earthquake point of view, nonductile RC frames were lack of ductility and energy dissipation.

Some scholars [1–9] have studied the seismic performance of nonductile frame structures and corrugated steel plate shear walls. Wu et al. [10] developed a multiscale model of nonductile frame. The hysteresis curves and skeleton curves of nonductile frame were analyzed by the developed model. The results showed that the multiscale model can simulate the boundary conditions of concrete components. Sae-Long et al. [11] proposed a fiber frame element for nonductile RC columns. The results revealed the essence of inclusion of shear response and shear flexure interaction. Shoraka et al. [12] introduced advanced analytical models to simulate the nonlinear dynamic response of nonductile RC structures. It estimated the expected losses of existing nonductile concrete buildings considering their vulnerability to collapse. The results showed that collapse did not occur in low earthquake shaking intensities and losses were dominated by nonstructural damage. It was effective to use the method of earthquake vulnerability.

On the basic of the researches, it was necessary to reinforce nonductile RC frame structures. At present, there were two main forms of reinforcements. One was steel bracing, and another one was carbon fiber reinforced plastic (CFRP). Song et al. [13] proposed shape memory alloy (SMA) braces. The nonlinear dynamic analyses and hysteresis performance of the SMA braces were studied. The results indicated that SMA braces strengthening nonductile concrete structures dissipated earthquake energy effectively. Khampanit [14] researched buckling-restrained braces reinforcing nonductile RC frames. An experiment and numbers of dynamic analyses were carried to verify the effectiveness of buckling-restrained braces. The researchers showed that this kind of braces enhanced stiffness, lateral force capacity, and energy dissipation of nonductile RC frames. Sarno and Manfredi [15] studied buckling-restrained braces (BRBs) to reinforce nonductile RC frames. Seven code-compliant natural earthquake records were selected and employed to perform inelastic response history analyses at serviceability. The results of analysis indicated that more than 60% of input seismic energy was dissipated by the BRBs at ultimate limit states. Chen et al. [16] conducted a study on a 1/2 scale two-span and two-storey specimen. The experiment was to research CFRP reinforced nonductile RC frames. The results showed that the average displacement ductility factor of retrofitted RC frame is 2.81. There was a large safety stock space when the maximum storey drift ratio reaches 1/50. Lv et al. [17] considered three reinforcement schemes about fiber reinforced polymer (FRP) rehabilitation. It compared seismic collapse fragilities between nonductile RC frames and reinforced specimens. The results showed that FRP rehabilitation scheme strengthening the entire structure promoted the seismic collapse resistance effectively.

The objective of this research is to study the reinforcement effect of corrugated steel plate shear walls slotted with columns. The paper changed parameter types (such as slit width, thickness, concrete strength, and boundary conditions) and compared seismic performance at different conditions.

The significance of this research is to propose corrugated steel plate shear walls reinforcing nonductile RC frames, which were separated with columns. The corrugated steel plate shear walls generate large oblique tension after buckling. This force extends to the surrounding RC beam and column members. The columns will bear the resulting transverse tension. As a result, the corresponding additional bending stress was generated in RC columns. To avoid the negative effect of steel plate tension belt on the RC frame columns, the corrugated steel plate shear was slotted with columns and connected with beams only.

2. Establishment of Nonductile RC Frame

2.1. Specimens Design. Two specimens of nonductile RC frame (ND-1, N is present non; *D* is present ductile) and nonductile RC frame retrofitted by corrugated steel plate shear walls slotted with columns (ND-2) were designed with the same dimensions and steel skeletons as shown in Figure 1. The reduced scale was 1/2. The clear span was 2.7 m, storey height was 1.8 m, and the total height was 2.65 m. The cross sections of column and beams were 180×200 mm, 150×250 mm, and 400×400 mm, respectively. The specimens were designed as nonductile frames. One of the standards about nonductile frame was insufficient transversal ties. Hence, it did not consider the joint area with dense transversal ties reinforcement.

Specimen ND-2 was reinforced by corrugated steel plate shear walls. The layout of corrugated steel plate shear walls is shown in Figure 2. The selected slit width was 10 mm. Corrugated steel plate shear walls were arranged on both sides of the frame. Corrugated steel plate shear walls were connected with beams using angle steel and tapping screws. The slabs of two pieces of corrugated steel plate shear walls were distributed as the shape of "X". As the reason of the limitation of plate width, rivets were adopted to connect two corrugated steel plate shear walls.

The connection method of corrugated steel plate shear walls and beams meets the demand of practical engineering. To research the influence of various factors of slotting with columns, the study of corrugated steel plate shear walls reinforced method is at the stage of finite element analysis at present.

2.2. Materials. Concrete average compressive strength was 30 MPa. The elasticity modulus of concrete was 30000 MPa. The diameter of longitudinal bars was 10 mm. Yield strength was 400 MPa. The diameter of transversal ties was 6 mm. Yield strength was 235 MPa. The elasticity modulus of longitudinal bars was 200000 MPa. The elasticity modulus of transversal ties was 210000 MPa. The yield strength corrugated steel plate of YX21-180-900 with 0.6 mm thickness was 264 MPa. Cross section dimensions of corrugated steel plate are shown in Figure 3. The properties of concrete, longitudinal bars, transversal ties, and corrugated steel plate are summarized in Table 1.

2.3. Loading Program and Boundary Conditions. The vertical load applied to the two columns was 51.48 kN. Axial compression ratio was $N/f_cA = 0.1$. Low cyclic loads were applied at the end of the beam and the loading program can be seen in Figure 4. The loading program was as per Qiu [18]. It indicated that one of the load rules was displacement-controlled loading. This load rule was also suitable for simulation. Considering the convergence of models, each load step had one cycle at a time. The bottom of two columns was rigid coupling. Vertical loads were applied as the form of area loads. The beam end was coupled for cycle loading.

The element of reinforced concrete is SOLID 65. The steel bars are dispersed in the concrete. The element of corrugated steel plate shear wall is SHEEL 181. The contact between elements is via the common nodes by cutting. The model is 3D. The boundary conditions at the base of the corrugated plates are solid joint.

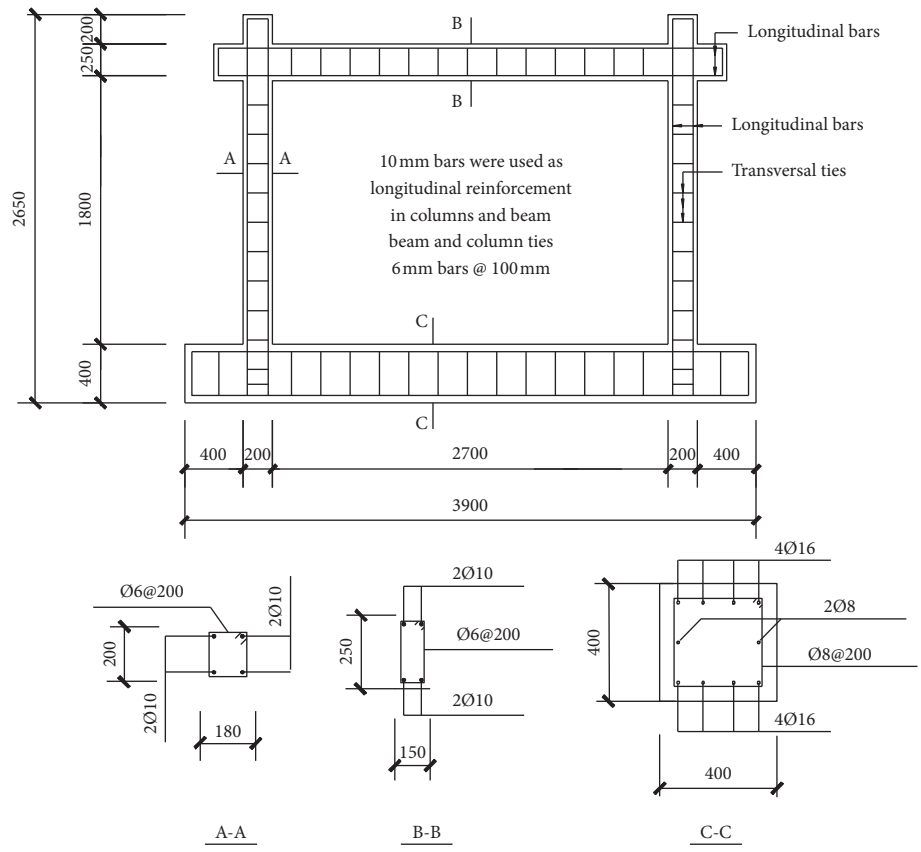

Figure 1: Steel skeletons.

2.4. Constitutive Model. On the basis of existing research, our team had published [19] about the material modes including concrete model, steel bar model, and corrugated steel plate model. The concrete model had an ascending part and descending part, which are shown in Figure 5. The steel bar and steel plate model was divided into two straight lines. In other words, the stress was close to ideal plasticity in a large deformation after reaching the yield strength. Steel bar and corrugated steel plate model are shown in Figure 6.

2.5. Verification of Finite Element Models. Our team [19] had verified the finite element model through comparing the hysteretic curves and skeleton curves of experimental and finite element results. The deviation of peak loads was 0.88% and 1.92%, respectively.

2.6. Finite Element Modeling of Nonductile RC Frame. Based on the verification of finite element models, the paper established the seismic behavior of nonductile RC frame retrofitted by corrugated steel plate shear walls slotted with columns only. The nonductile RC frame (ND-1) and the reinforced frame (ND-2) are shown in Figures 7(a) and 7(b). Slit width of Specimen ND-2 was 10 mm.

3. Analysis Results

3.1. Strength and Ductility. The hysteretic curves and skeleton curves of Specimen ND-1 and Specimen ND-2 are shown in Figures 8 and 9. The yield load, ultimate load, displacements, and ductility can be seen in Table 2. It indicated that the strength had been improved 100.76% when the nonductile RC frame was strengthened with corrugated steel plate shear walls. The ductility was improved from 2.86 to 3.67.

3.2. Stiffness. The stiffness curves of Specimen ND-1 and Specimen ND-2 are shown in Figure 10. The initial stiffness and ultimate stiffness can be seen in Table 3. It showed that the initial stiffness and ultimate stiffness had been enhanced by 63.85% and 38.26%. The stiffness had been improved greatly.

3.3. Energy Dissipating Capacity. The accumulated energy dissipation curves of Specimen ND-1 and Specimen ND-2 are shown in Figure 11. It showed that the accumulated energy dissipation of Specimen ND-1 and Specimen ND-2 was 1602.26 kN mm and 10138.14 kN mm. The energy dissipation improved by 84.20%.

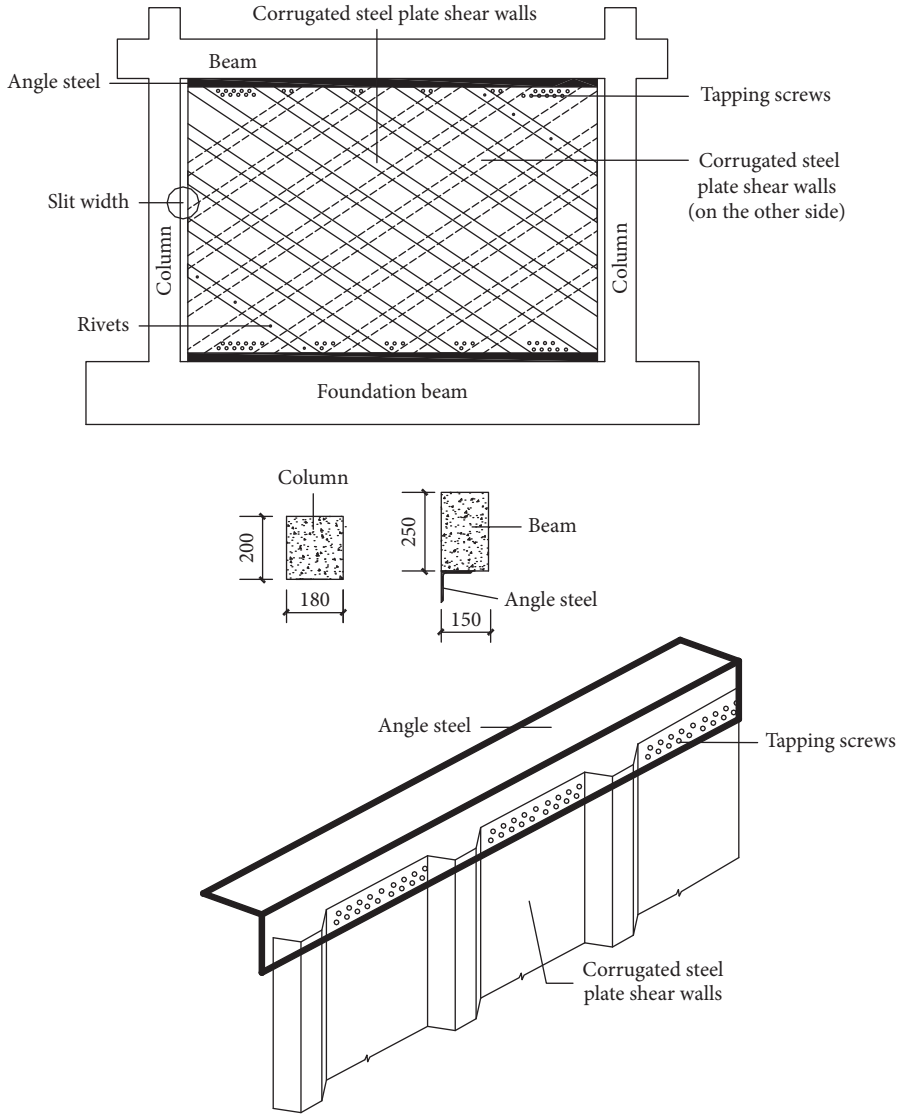

Figure 2: Arrangement diagram.

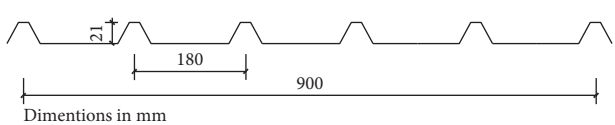

Figure 3: Cross section dimensions of corrugated steel plate.

Table 1: Material properties.

Materials	Concrete compressive strength $f_{cu,k}$ (MPa)	Yield strength f_y (MPa)
Concrete	30	—
Longitudinal bars	—	400
Transversal ties	—	235
Corrugated steel plate	—	264

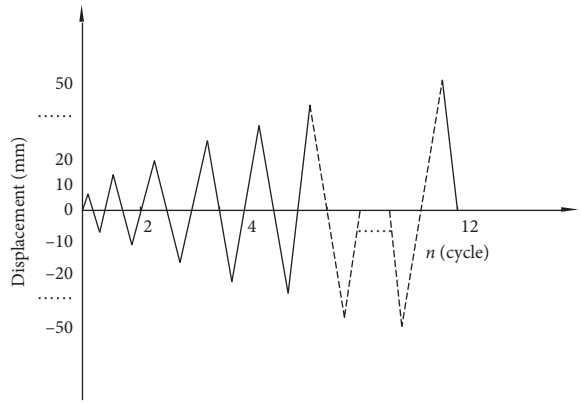

Figure 4: Loading program.

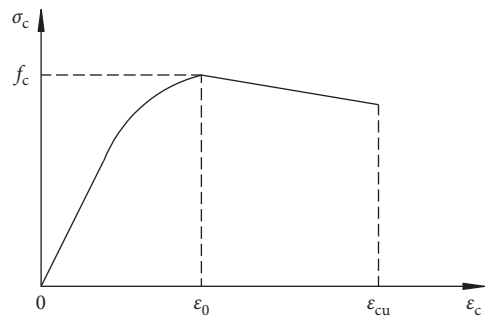

Figure 5: Concrete model.

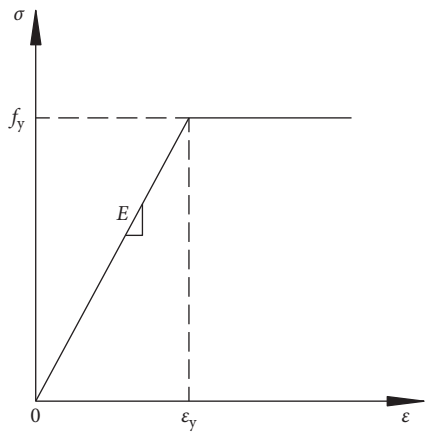

Figure 6: Steel bar and corrugated steel plate model.

4. Parameters Analysis

The paper discussed 24 specimens (ND-1–ND-24) in different influence parameters. The influence parameters are listed in Table 4. It can be seen from the table that the slit width was composed of 5 mm, 10 mm, 20 mm, 30 mm, 40 mm, 60 mm, 100 mm, 200 mm, 300 mm, and 400 mm. The selected slit width was on the basis of Zhao [20] team research. The thickness of corrugated steel plate shear walls was divided into 0.4 mm, 0.6 mm, and 0.8 mm. The selected thickness was in the light of experiments and finite element analysis [19, 21]. The concrete compressive strength of nonductile RC frame was 30 MPa, 40 MPa, 50 MPa, and 60 MPa, respectively. Boundary conditions of corrugated steel plate shear walls at slotted parts were divided into two parts: Z-direction constraint and without constraint.

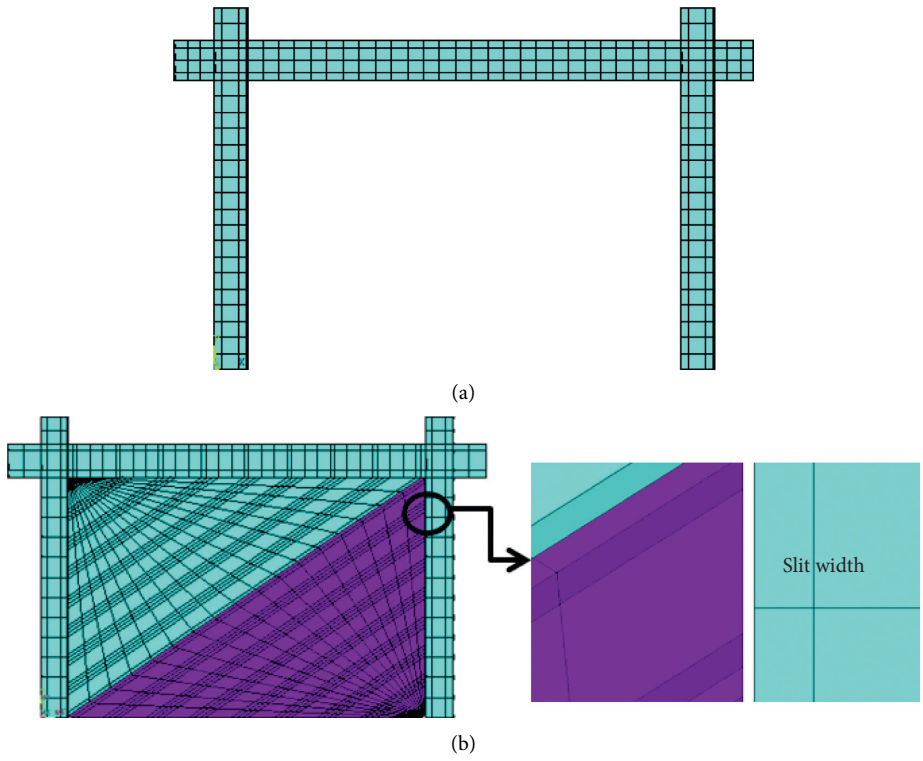

Figure 7: Finite element models. (a) Nonductile RC frame (ND-1). (b) Reinforced frame (ND-2) with slit width (10 mm).

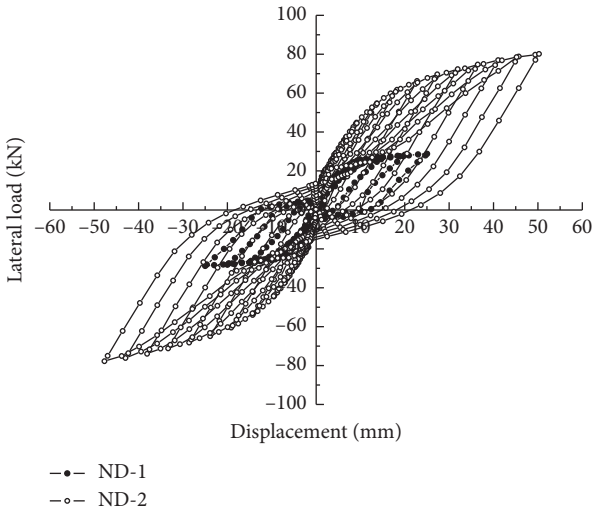

Figure 8: Hysteretic curves.

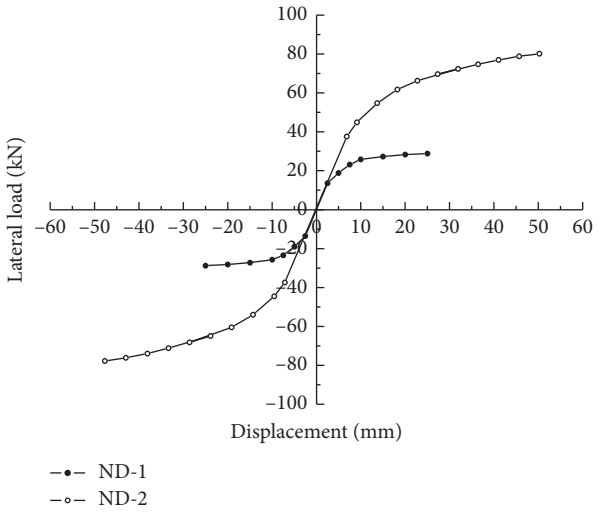

Figure 9: Skeleton curves.

5. Discussion

Hysteretic curves, skeleton curves, ductility, and stiffness are discussed in this section. The influence parameters are slit width, thickness, concrete strength, and boundary conditions. As can be seen in Table 4, the paper selected ND-2, ND-16, ND-18, and ND-24 corresponding slit widths 10 mm, 100 mm, 200 mm, and 400 mm to analyze the influence of slit width on the whole structure. Specimens ND-1, ND-2, ND-3, ND-15, ND-16, and ND-17 were selected to compare the influence of thickness. Specimens ND-11, ND-12, ND-13, ND-14, ND-18, ND-19, ND-20, and ND-21 were chosen to compare the effect of concrete strength of the structure. Boundary conditions of corrugated steel plate edge at slotted parts were related Specimens ND-5, ND-6, ND-7, ND-8, ND-9, ND-10, ND-22, and ND-23. The selected slit width was on the basis of Zhao [20] team research. The thickness of corrugated steel plate shear walls was divided into 0.4 mm, 0.6 mm, and 0.8 mm. The selected thickness was in the light of experiments and

Table 2: Loads, displacement, and ductility.

Specimen	Slit width (mm)	Yield load (kN)	Δ_y (mm)	Ultimate load (kN)	Δ_u (mm)	Ductility
ND-1	—	23.95	8.76	28.86	25.03	2.86
ND-2	10	54.72	13.69	80.10	50.25	3.67

Δ_y: yield displacement; Δ_u: ultimate load.

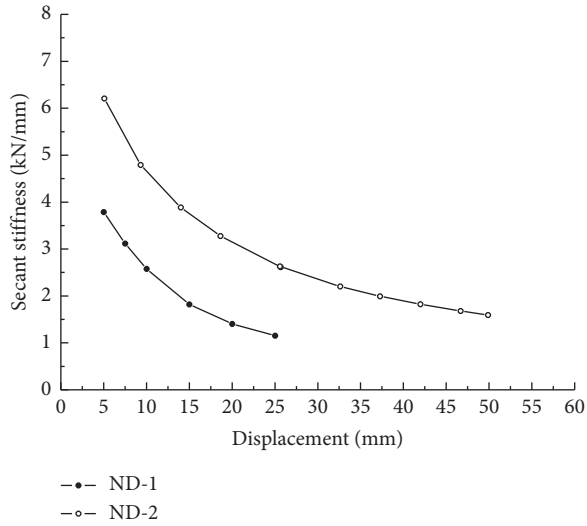

Figure 10: Stiffness curves.

Table 3: Initial stiffness and ultimate stiffness.

Specimen	Slit width (mm)	Initial stiffness (kN/mm)	Ultimate stiffness (kN/mm)
ND-1	—	3.79	1.15
ND-2	10	6.21	1.59

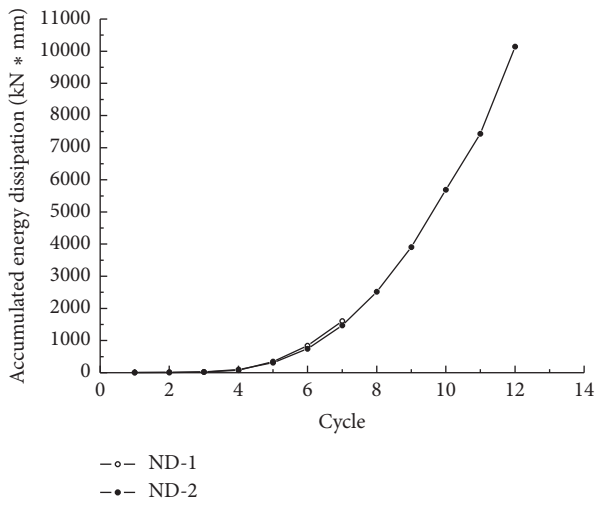

Figure 11: Accumulated energy dissipation.

finite element analysis [19, 21]. The reason for selecting big difference slit width was to contrastively analyze the mechanical property under the big difference slit width from Section 5.1 to Section 5.4.

5.1. Slit Width

5.1.1. Hysteretic Curves. The hysteretic curves of different slit width are shown in Figures 12(a)–12(d). It can be seen from the figures that the hysteretic curves were not full while the slit width was larger. In the other words, the plump degree declined with the increase of corrugated steel plate width. It manifested that corrugated steel plate shear walls slotted with columns could achieve good dissipation capacity. When the slit width was within the scope of 200 mm, the energy dissipating could gain good performance.

5.1.2. Skeleton Curves. The skeleton curves of different slit width are shown in Figure 13. Loads, displacement, and ductility of different slit width are listed in Table 5. The skeleton curves had the same trend. Because of the convergence of finite element models, the paper compared different strength under the displacement of about 50 mm. The skeleton curves derived from the maximum load and displacement of each hysteretic loop and the yield loads and ultimate loads are listed in Table 3. It can be derived from the table that the ultimate loads were 80.10 kN, 56.73 kN, 50.27 kN, and 38.48 kN and the corresponding slit widths

Table 4: Influence parameters.

Specimens	Slit width (mm)	Thickness (mm)	Concrete strength (MPa)	Boundary conditions
ND-1	5	0.4	30	—
ND-2		0.6		
ND-3		0.8		
ND-2	10	0.6	30	—
ND-5	20	0.6	30	UZ
ND-6				—
ND-7	30	0.6	30	UZ
ND-8				—
ND-9	40	0.6	30	UZ
ND-10				—
ND-11	60	0.6	30	—
ND-12			40	
ND-13			50	
ND-14			60	
ND-15	100	0.4	30	—
ND-16		0.6		
ND-17		0.8		
ND-18	200	0.6	30	—
ND-19			40	
ND-20			50	
ND-21			60	
ND-22	300	0.6	30	UZ
ND-23				—
ND-24	400	0.6	30	—

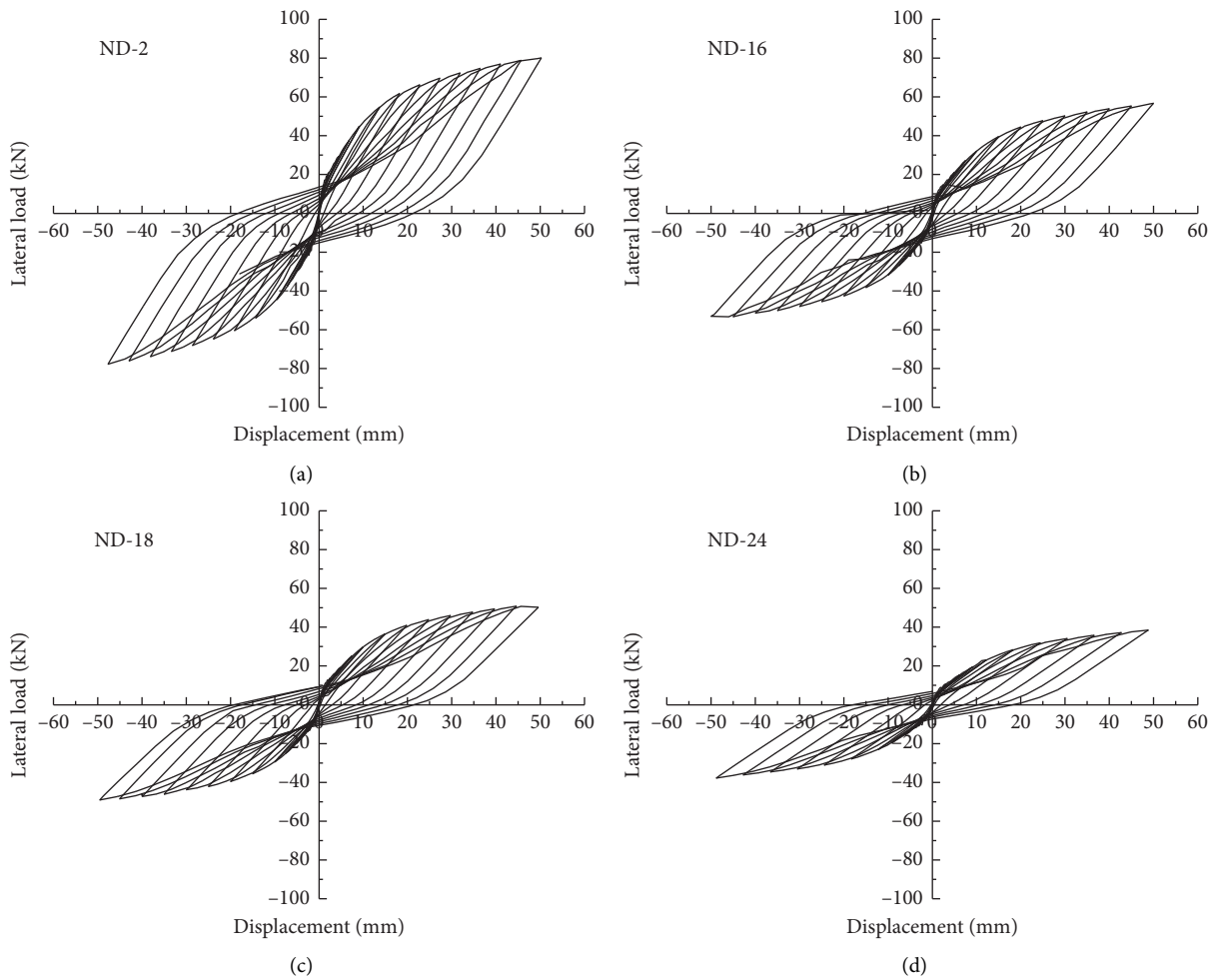

Figure 12: Hysteretic curves of different slit width. (a) 10 mm. (b) 100 mm. (c) 200 mm. (d) 400 mm.

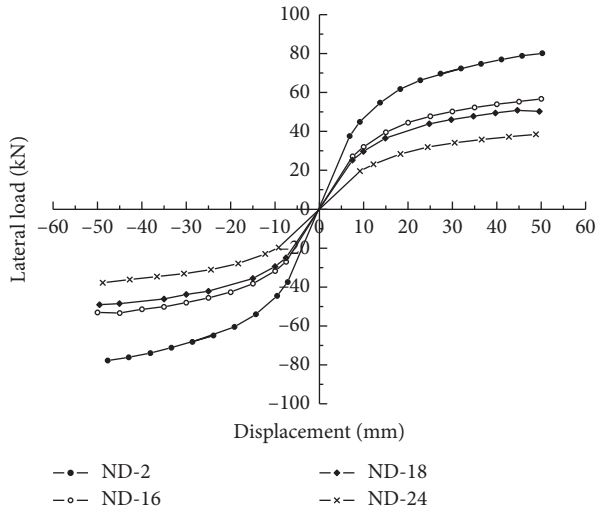

Figure 13: Skeleton curves of different slit width.

Table 5: Loads, displacement, and ductility of different slit width.

Specimen	Slit width (mm)	Yield load (kN)	Δ_y (mm)	Ultimate load (kN)	Δ_u (mm)	Ductility
ND-2	10	54.72	13.69	80.10	50.25	3.67
ND-16	100	39.56	15.23	56.73	50.01	3.28
ND-18	200	37.86	15.22	50.27	49.57	3.26
ND-24	400	26.07	15.34	38.48	48.80	3.18

Δ_y: yield displacement; Δ_u: ultimate load.

were 10 mm, 100 mm, 200 mm, and 400 mm, respectively. The strength declined witg the increase of the slit width.

5.1.3. Ductility. The ductility of different slit width can be seen in Table 5. The ductility was 3.67, 3.28, 3.26, and 3.18, respectively. The value of ductility was above 3.0, which indicated that nonductile RC frame retrofitted by corrugated steel plate shear walls slotted with columns gained enough ductility.

5.1.4. Stiffness Curves. The stiffness curves of different slit width are presented in Figure 14. The initial stiffness and ultimate stiffness of different slit width are presented in Table 6. When the slit width was 10 mm, the structure gained greater initial stiffness. When the slit width was in the scope of 100 mm–200 mm, the stiffness was closely relatively and decreased somewhat. The initial stiffness decreased largely when the slit width changed into 400 mm.

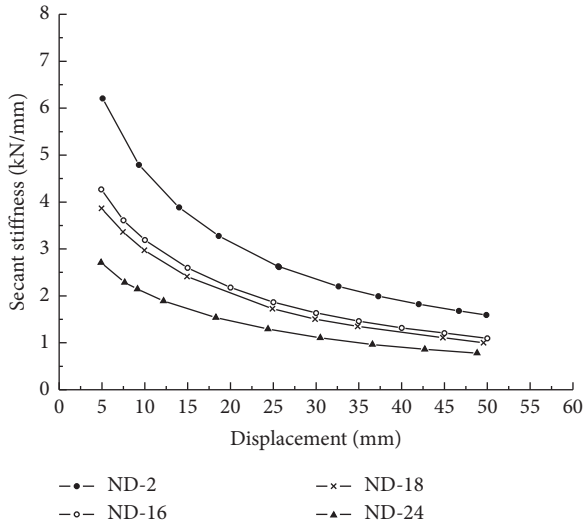

Figure 14: Stiffness curves of different slit width.

5.2. Thickness

5.2.1. Hysteretic Curves. The paper selected slit widths 5 mm and 100 mm to investigate the influence of thickness. The thicknesses were 0.4 mm, 0.6 mm, and 0.8 mm. The hysteretic curves of slit widths 5 mm and 100 mm are shown in Figures 15(a)–15(c) and 16(a)–16(c). Figures showed that the strength was improved with the increase of thickness. The energy dissipation had been enhanced when the thickness increased.

5.2.2. Skeleton Curves. The skeleton curves of slit widths 5 mm and 100 mm are shown in Figures 17 and 18. Loads, displacement, and ductility of different thickness are listed in Table 7. When the slit width was 5 mm, the ultimate loads of

Table 6: Stiffness of different slit width.

Specimen	Slit width (mm)	Initial stiffness (kN/mm)	Ultimate stiffness (kN/mm)
ND-2	10	6.21	1.59
ND-16	100	4.27	1.10
ND-18	200	3.87	1.01
ND-24	400	2.71	0.78

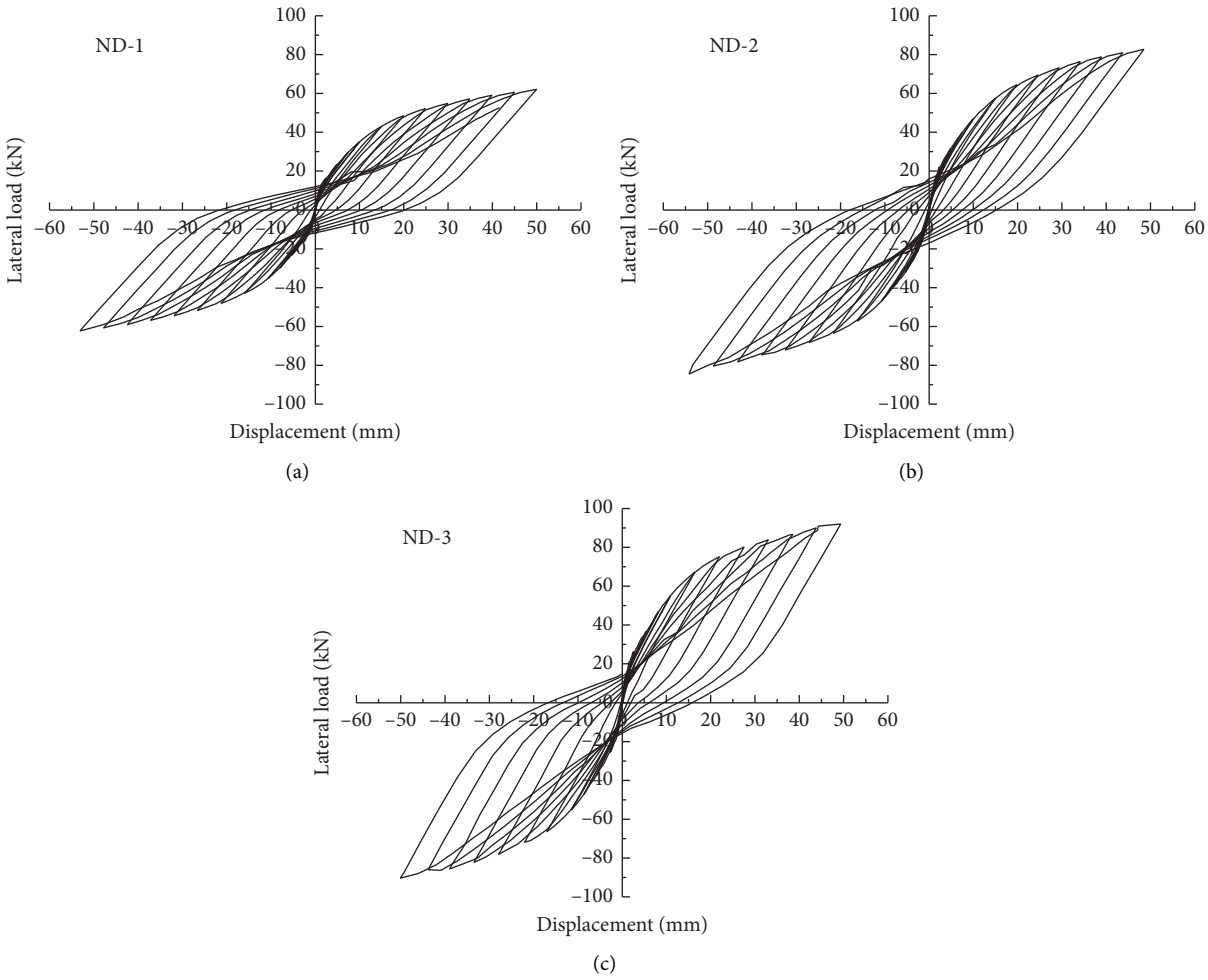

Figure 15: Hysteretic curves of slit width 5 mm. (a) 0.4 mm. (b) 0.6 mm. (c) 0.8 mm.

thickness 0.6 mm and 0.8 mm were improved by 34.15% and 53.03% compared to that of thickness 0.4 mm, respectively. When the slit width was 100 mm, the ultimate loads of thicknesses 0.6 mm and 0.8 mm were improved by 44.20% and 78.55% compared to that of thickness 0.4 mm, respectively.

5.2.3. Ductility. The ductility of different thickness can be seen in Table 7. It can be seen from the table that the ductility was enhanced with the increase of thickness. When the slit width was 5 mm, the ductility was from 4.19 to 4.52. When the slit width was 100 mm, the ductility was from 3.24 to 3.34. It indicated that the space between the columns and corrugated steel plate shear walls worked and gained good ductility. The columns were protected from the additional bending moment and axial force of corrugated steel plate shear walls.

5.2.4. Stiffness Curves. The stiffness curves of slit width 5 mm and 100 mm are presented in Figures 19 and 20. The initial stiffness and ultimate stiffness of different thickness are presented in Table 8. The thickness 0.8 mm obtained larger stiffness than thickness 0.6 mm and 0.4 mm. Initial stiffness of thickness 0.6 mm was improved by 35.50% and 45.73% than that of thickness 0.4 mm. Initial stiffness of thickness 0.8 mm was improved by 44.59% and 89.41% than that of thickness 0.4 mm. It showed that nonductile RC frame retrofitted by corrugated steel plate shear walls slotted

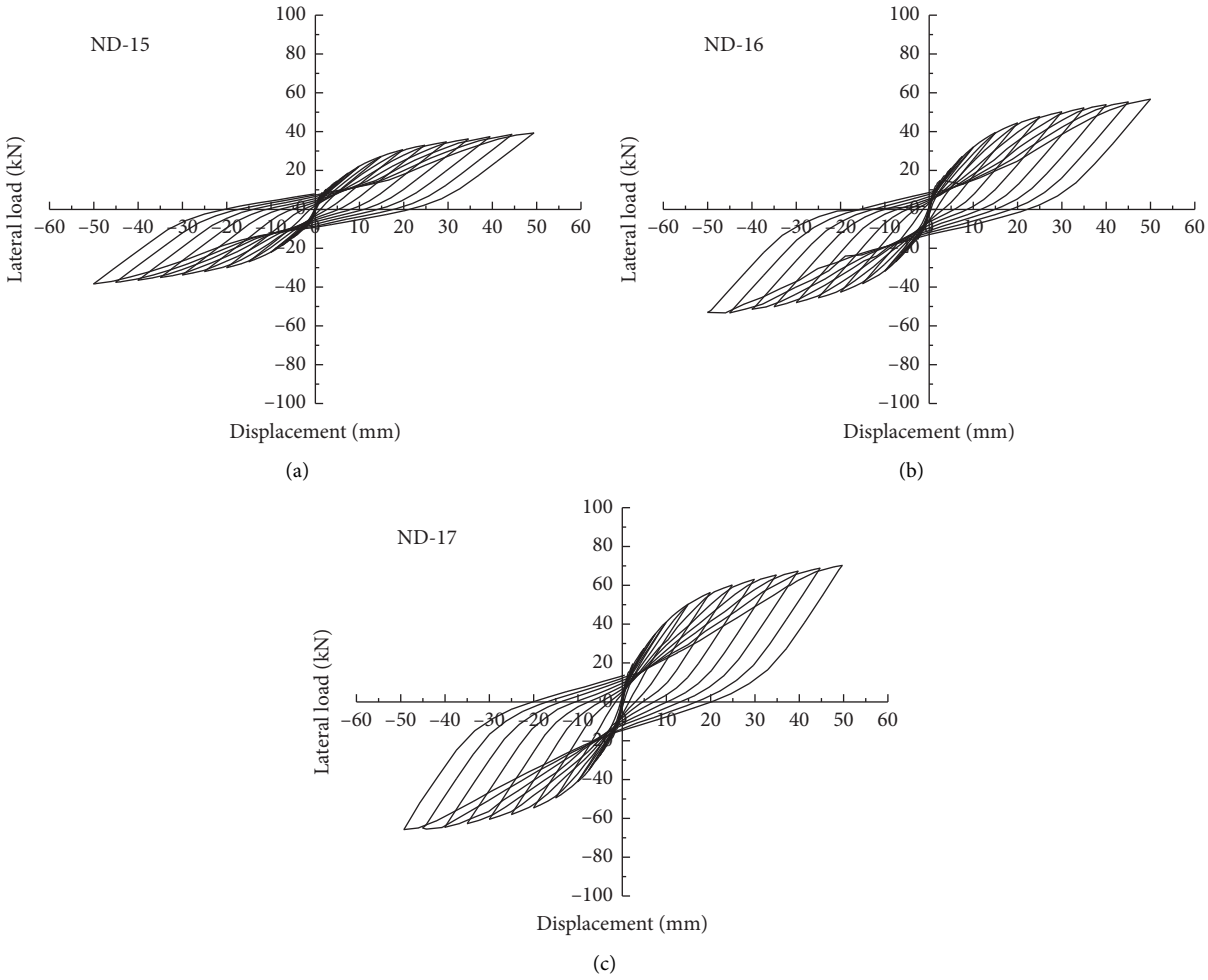

Figure 16: Hysteretic curves of slit width 100 mm. (a) 0.4 mm. (b) 0.6 mm. (c) 0.8 mm.

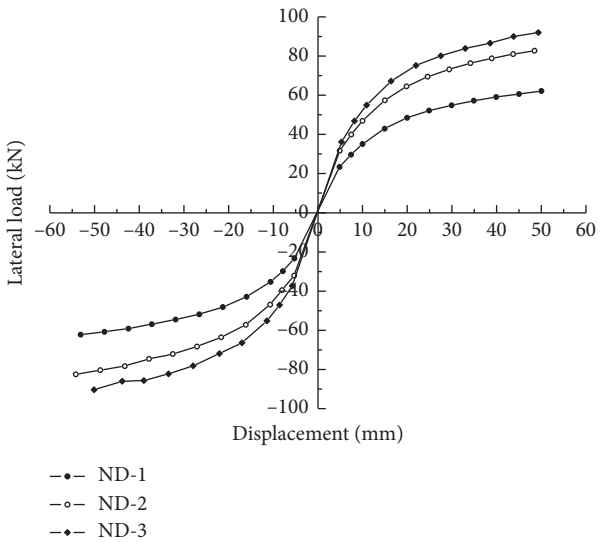

Figure 17: Skeleton curves of slit width 5 mm.

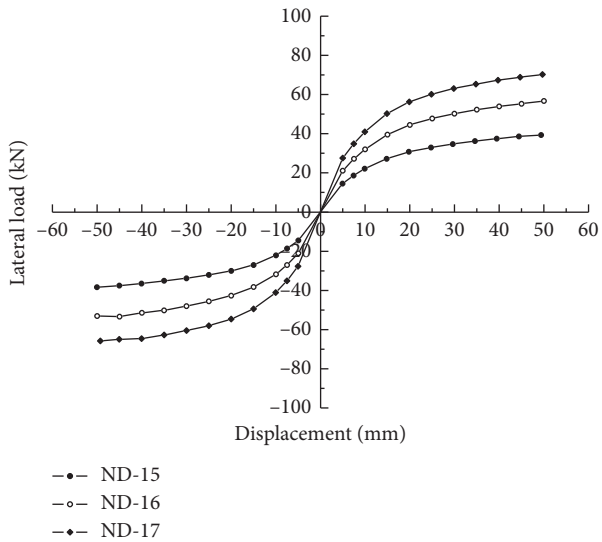

Figure 18: Skeleton curves of slit width 100 mm.

Table 7: Loads, displacement, and ductility of different thickness.

Specimen	Slit width (mm)	Thickness	Yield load (kN)	Δy (mm)	Ultimate load (kN)	Δu (mm)	Ductility
ND-1	5	0.4	38.97	11.92	60.14	49.99	4.19
ND-2	5	0.6	49.45	10.97	80.68	48.49	4.42
ND-3	5	0.8	55.02	10.92	92.03	49.35	4.52
ND-15	100	0.4	28.21	15.25	39.34	49.35	3.24
ND-16	100	0.6	39.56	15.23	56.73	50.01	3.28
ND-17	100	0.8	50.3	14.89	70.24	49.66	3.34

Δ_y: yield displacement; Δ_u: ultimate load.

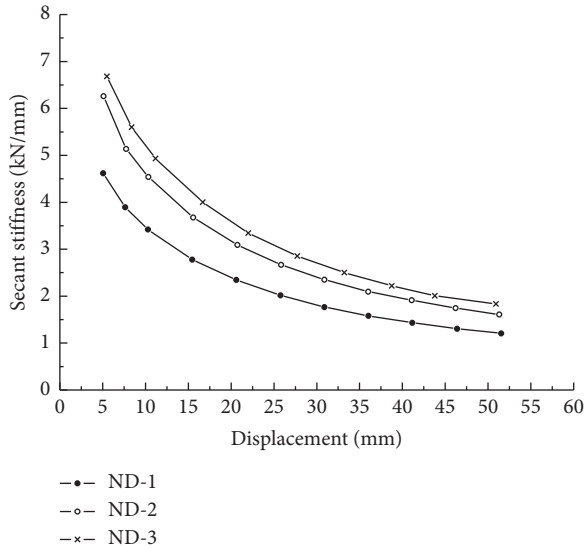

Figure 19: Stiffness curves of slit width 5 mm.

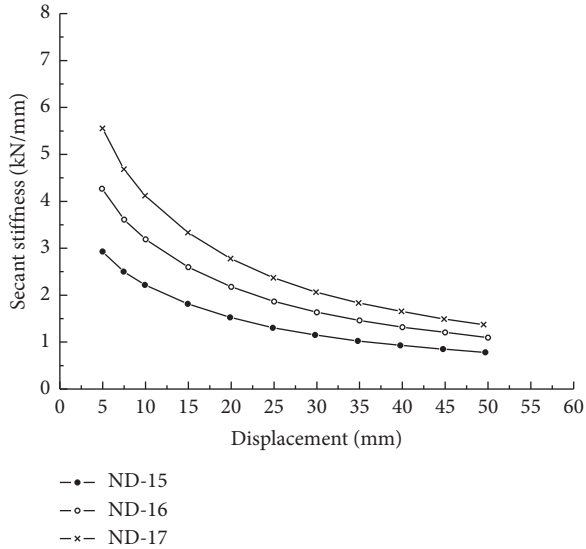

Figure 20: Stiffness curves of slit width 100 mm.

Table 8: Stiffness of different thickness.

Specimen	Slit width (mm)	Thickness (mm)	Initial stiffness (kN/mm)	Ultimate stiffness (kN/mm)
ND1	5	0.4	4.62	1.21
ND2	5	0.6	6.26	1.61
ND3	5	0.8	6.68	1.83
ND15	100	0.4	2.93	0.78
ND16	100	0.6	4.27	1.10
ND17	100	0.8	5.55	1.38

with columns only can be gained good stiffness. With the increase of thickness, the stiffness was enhanced largely.

5.3. Concrete Strength

5.3.1. Hysteretic Curves. The paper chose slit width 60 mm and 200 mm to investigate the influence of concrete strength. The concrete strength was 30 MPa, 40 MPa, 50 MPa and 60 MPa. The hysteretic curves of slit width 60 mm and 200 mm are shown in Figures 21(a)–21(d) and 22(a)–22(d). Figures showed that the strength was improved as the increase of concrete strength. The energy dissipation had been enhanced when the concrete strength increased.

5.3.2. Skeleton Curves. The skeleton curves of slit width 60 mm and 200 mm are shown in Figures 23 and 24. Loads, displacement and ductility of different concrete strength are listed in Table 9. When the slit width was 60 mm, the ultimate loads of concrete strength 40 MPa, 50 MPa and 60 MPa were improved by 10.69%, 27.80% and 39.64% than that of concrete strength 30 MPa, respectively. When the slit width was 200 mm, the ultimate loads of concrete strength 40 MPa, 50 MPa and 60 MPa were improved by 17.90%, 32.90% and 49.13% than that of concrete strength 30 MPa, respectively.

5.3.3. Ductility. The ductility of different concrete strength is presented in Table 9. It can be seen from the table that the ductility was enhanced with the increase of concrete strength. When the slit width was 60 mm, the ductility was from 3.42 to 3.62. When the slit width was 200 mm, the ductility was from 3.26 to 3.65. It indicated that the strengthened non-ductility RC frame earned good seismic performance in the scope of 60 MPa.

5.3.4. Stiffness Curves. The stiffness curves of slit width 60 mm and 200 mm are presented in Figures 25 and 26. The initial stiffness and ultimate stiffness of different concrete strength are presented in Table 10. The concrete strength 60 MPa had the largest initial stiffness 5.93 kN/mm and the concrete strength 30 MPa had the smallest initial stiffness 4.48 kN/mm when the slit width was 60 mm. The concrete strength 60 MPa had the largest initial stiffness 5.32 kN/mm and the concrete strength 30 MPa had the smallest initial stiffness 4.32 kN/mm when the slit width was 200 mm. The stiffness was increased by 32.37% and 23.15%, respectively. It indicated that concrete strength influenced stiffness was not as large as the thickness parameter.

5.4. Boundary Conditions

5.4.1. Hysteretic Curves. The paper chose slit width 20 mm, 30 mm, 40 mm and 300 mm to study the influence of boundary conditions. The boundary conditions were with and without Z-direction constraint on the edge of corrugated steel plate shear walls. The hysteretic curves of slit width 20 mm, 30 mm, 40 mm and 300 mm are shown in Figures 27(a) and 27(b)–30(a) and 30(b). These figures indicated that the strength and energy dissipation were improved with Z-direction constraint. The Z-direction constrain transferred the internal shear better. It made better use of materials of the edge of corrugated steel plate shear walls.

5.4.2. Skeleton curves. The skeleton curves of slit width 20 mm, 30 mm, 40 mm and 300 mm are shown in Figures 31–34. Loads, displacement and ductility of different boundary conditions are listed in Table 11. When the slit width was 20 mm, the ultimate loads of Z-direction constrain was improved by 13.93% than that of non-constrain. When the slit width was 30 mm, the ultimate loads of Z-direction constrain was improved by 9.26% than that of non-constrain. When the slit width was 40 mm, the ultimate loads of Z-direction constrain was improved by 11.91% than that of non-constrain. When the slit width was 300 mm, the ultimate loads of Z-direction constrain was improved by 27.71% than that of non-constrain.

5.4.3. Ductility. The ductility of different boundary conditions is presented in Table 11. It can be seen from the table that the ductility was improved with Z-direction constrain. However, the enhancement was not so obvious. The improved range was 1.71%, 1.69%, 0.57% and 2.88%, respectively. It indicated that changing the boundary conditions had little effect on ductility.

5.4.4. Stiffness Curves. The stiffness curves of slit width 20 mm, 30 mm, 40 mm and 300 mm are presented in Figures 35–38. The initial stiffness and ultimate stiffness of different boundary conditions are presented in Table 12. It can be seen from the table that the Z-direction constraint was improved 13.23%, 13.81%, 7.80%, 27.49% than that of non-constraint, respectively. The trend of stiffness curves were in accordance with each other. The improved amplitude was not a large increase.

5.5. Explanation of Slotted Principle.

The proposed slotted principle was based on the following principles. When shear walls adopt plain plate, the shear buckling tends to occur at lower lateral forces. Then shear walls take lateral loads through oblique tension band action. The columns anchor the oblique tension band while the tension belt also causes a relatively high additional bending moment to the columns [22].

The proposed corrugated steel plate shear walls have ribs on the surface, which improves buckling strength prominently. It solves the buckling of plain plate easily. Through the analysis of each parameter in the paper, it can be seen that corrugated steel plate shear walls transmit force in the form of in-plane shear. The force form accords with the slotted principle. Strength, ductility, stiffness, and energy dissipating perform well within a reasonable slit range. The nonductile RC frame gained good seismic performance.

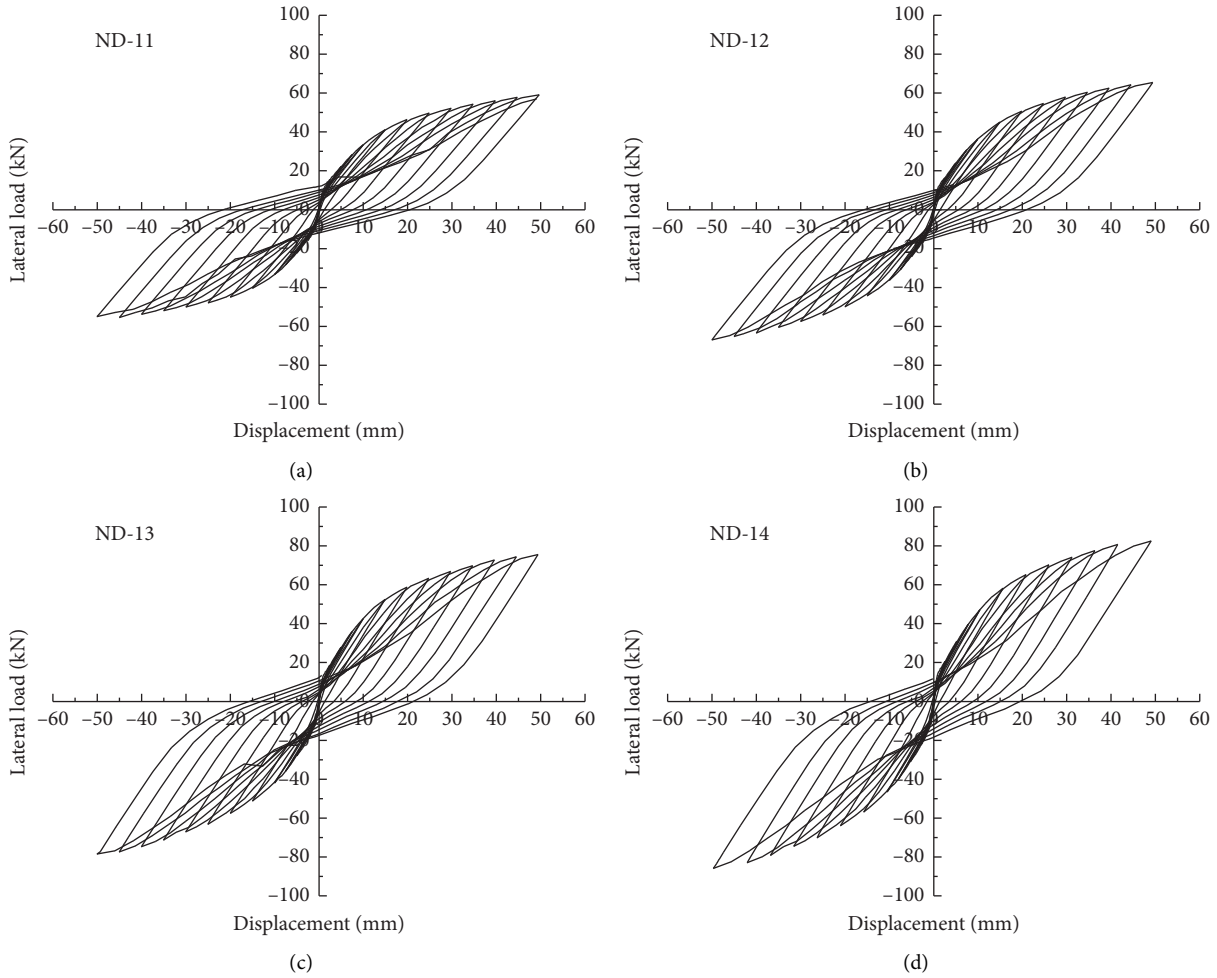

Figure 21: Hysteretic curves of slit width 60 mm. (a) 30 MPa. (b) 40 MPa. (c) 50 MPa. (d) 60 MPa.

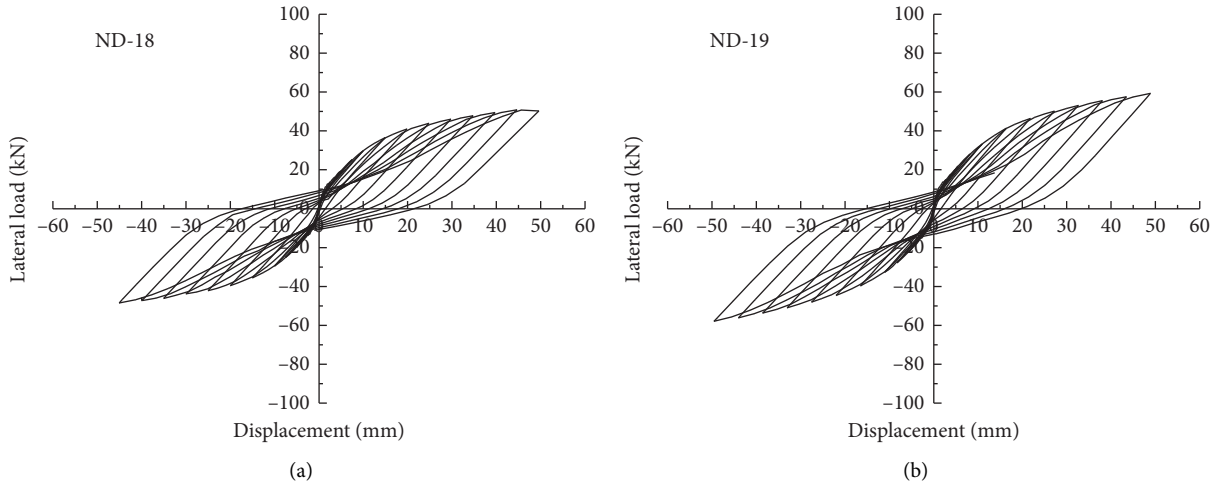

Figure 22: Continued.

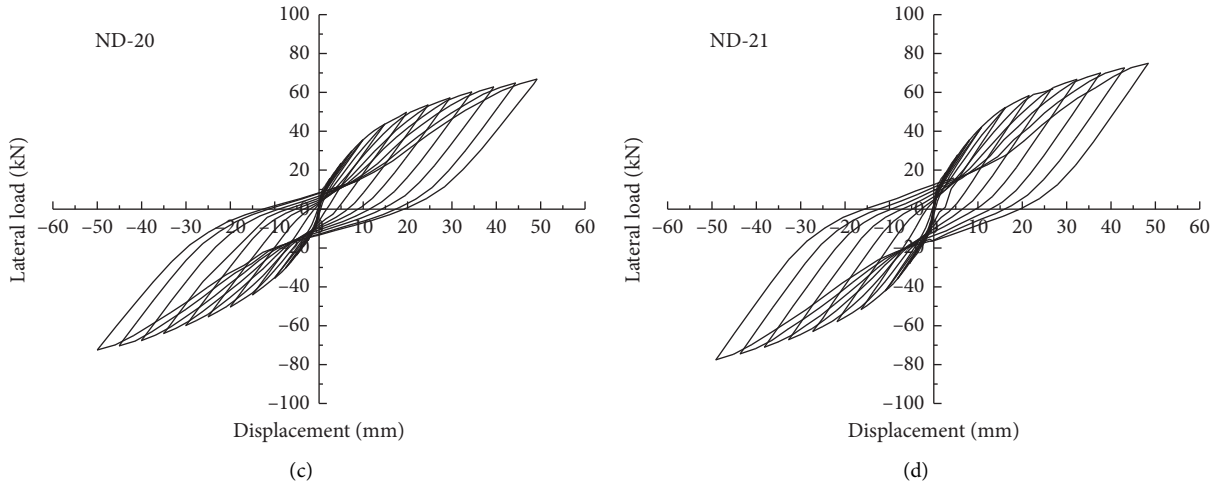

Figure 22: Hysteretic curves of slit width 200 mm. (a) 30 MPa. (b) 40 MPa. (c) 50 MPa. (d) 60 MPa.

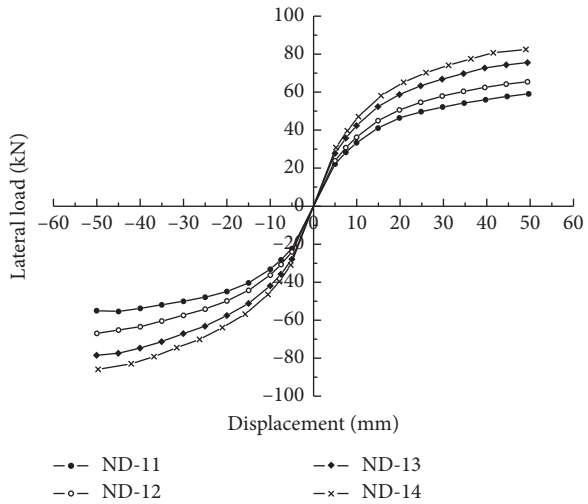

Figure 23: Skeleton curves of slit width 60 mm.

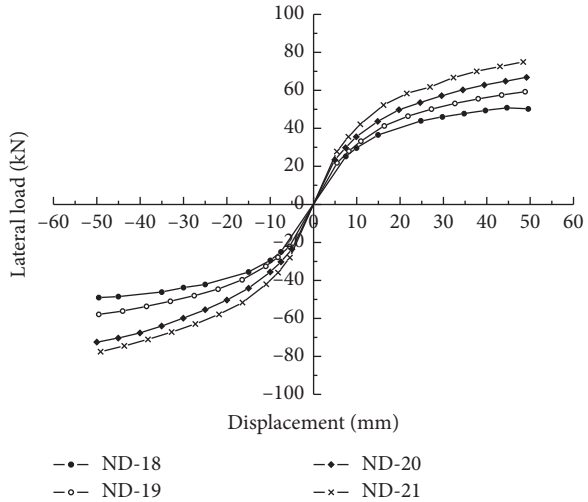

Figure 24: Skeleton curves of slit width 200 mm.

Table 9: Loads, displacement and ductility of different concrete strength.

Specimen	Slit width (mm)	Concrete strength (MPa)	Yield load (kN)	Δ_y (mm)	Ultimate load (kN)	Δ_u (mm)	Ductility
ND11	60	30	40.97	14.51	59.11	49.631	3.42
ND12	60	40	44.65	14.27	65.43	49.392	3.46
ND13	60	50	51.36	13.89	75.54	49.394	3.56
ND14	60	60	52.78	13.55	82.54	49.025	3.62
ND18	200	30	37.86	15.22	50.27	49.57	3.26
ND19	200	40	39.59	14.76	59.27	48.87	3.31
ND20	200	50	43.09	14.21	66.81	49.19	3.46
ND21	200	60	47.77	13.26	74.97	48.39	3.65

Δ_y: Yield displacement; Δ_u: Ultimate load.

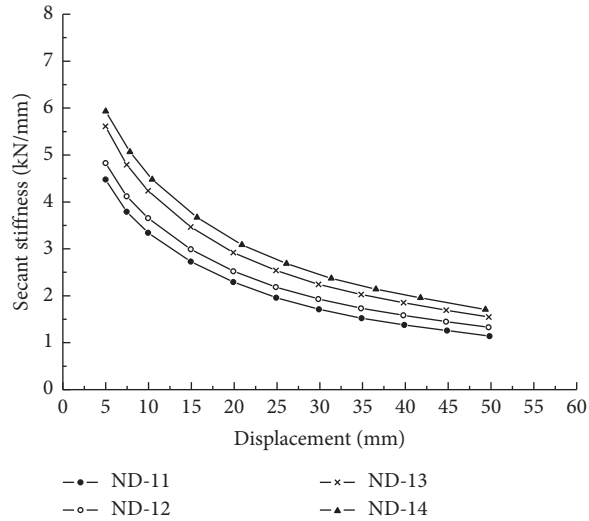

Figure 25: Stiffness curves of slit width 60 mm.

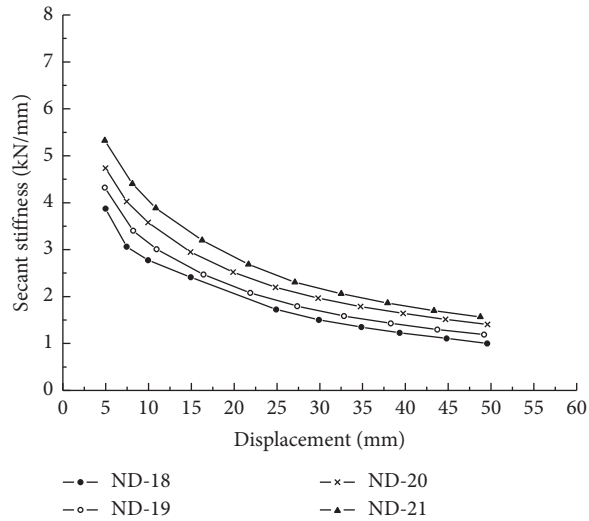

Figure 26: Stiffness curves of slit width 200 mm.

Table 10: Stiffness of different concrete strength.

Specimen	Slit width (mm)	Thickness (mm)	Initial stiffness (kN/mm)	Ultimate stiffness (kN/mm)
ND11	60	30	4.48	1.15
ND12	60	40	4.83	1.33
ND13	60	50	5.61	1.55
ND14	60	60	5.93	1.71
ND18	200	30	3.87	1.01
ND19	200	40	4.32	1.19
ND20	200	50	4.74	1.40
ND21	200	60	5.32	1.56

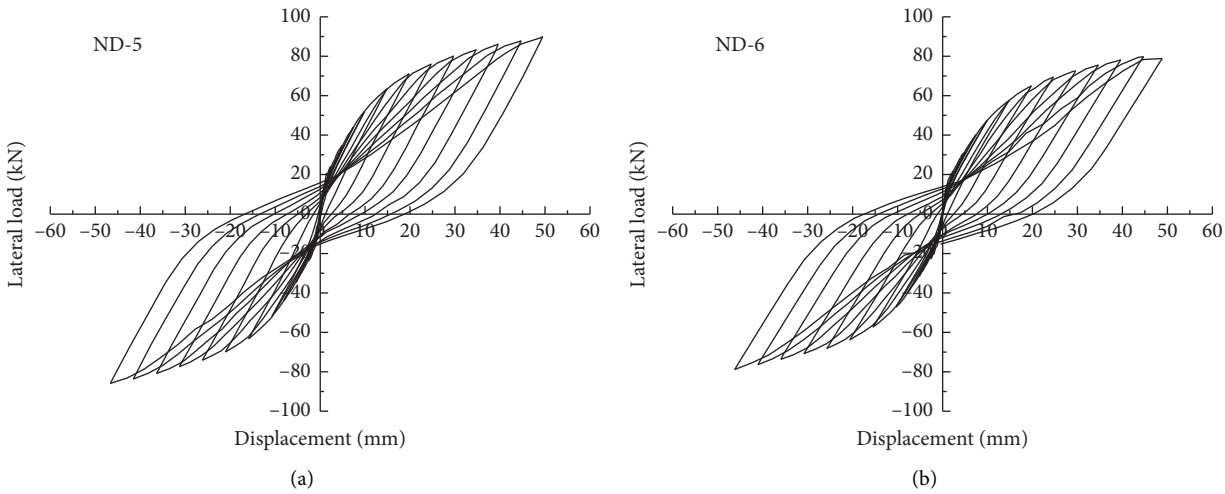

Figure 27: Hysteretic curves of Slit width 20 mm. (a) Z-direction constrain. (b) Without constrain.

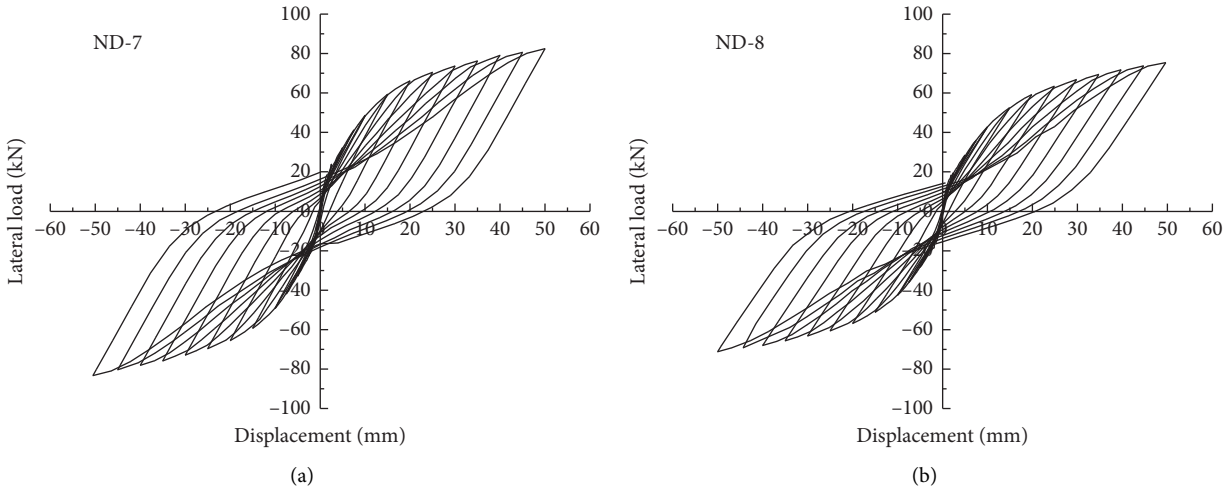

Figure 28: Hysteretic curves of Slit width 30 mm. (a) Z-direction constrain. (b) Without constrain.

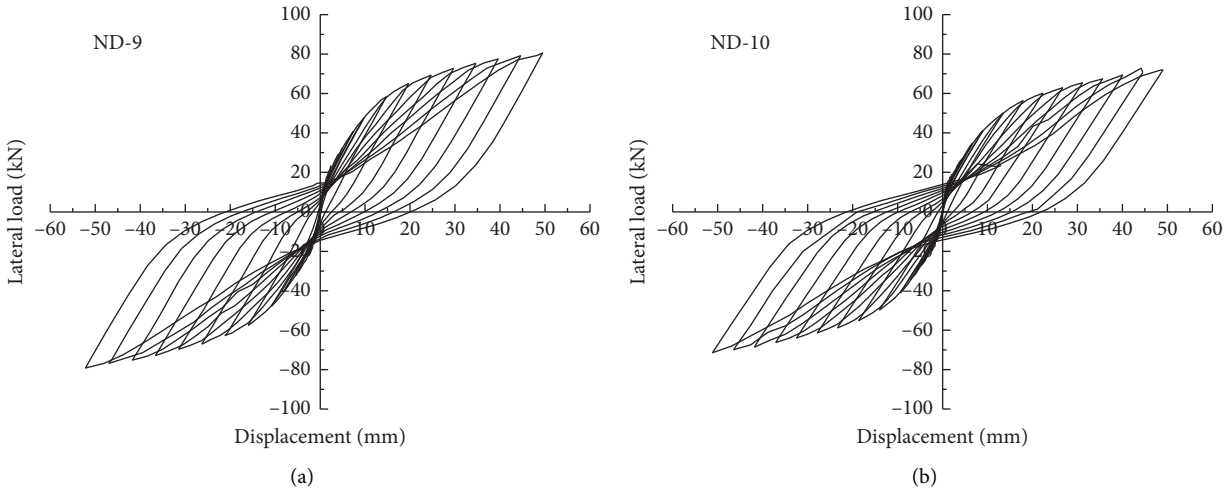

Figure 29: Hysteretic curves of Slit width 40 mm. (a) *Z*-direction constrain. (b) Without constrain.

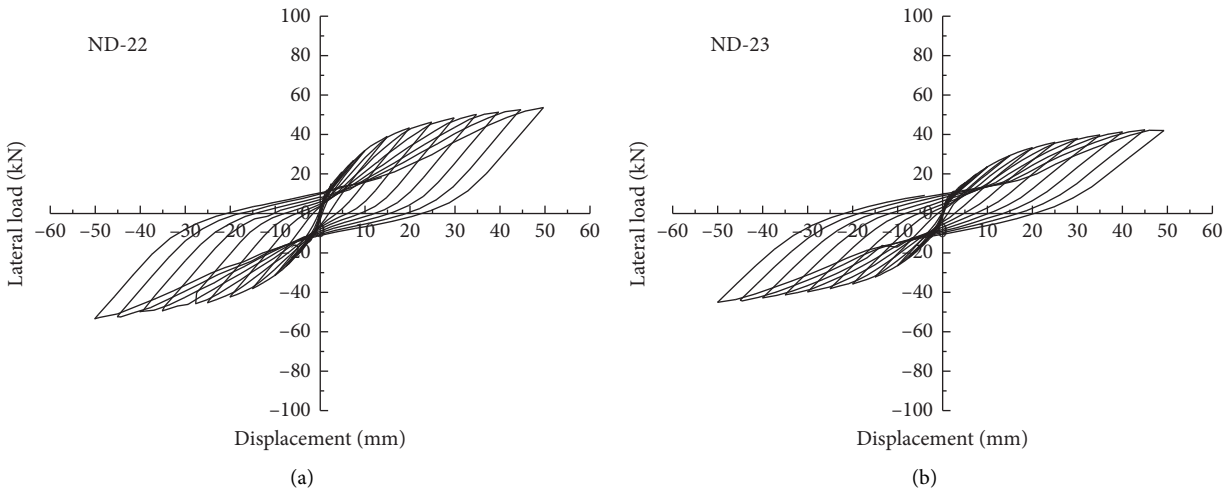

Figure 30: Hysteretic curves of Slit width 300 mm. (a) *Z*-direction constrain. (b) Without constrain.

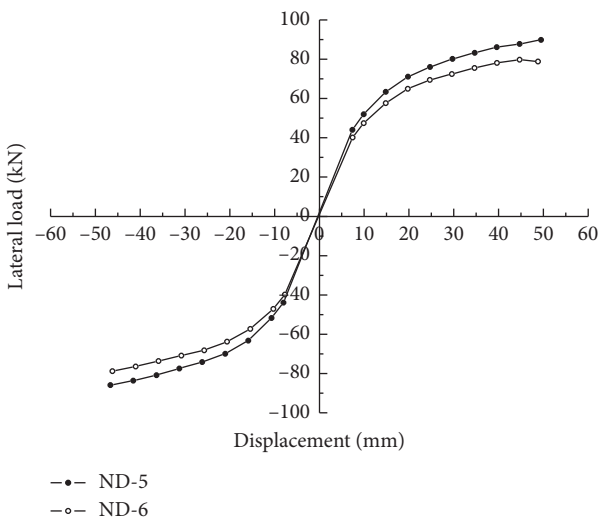

Figure 31: Skeleton curves of slit width 20 mm.

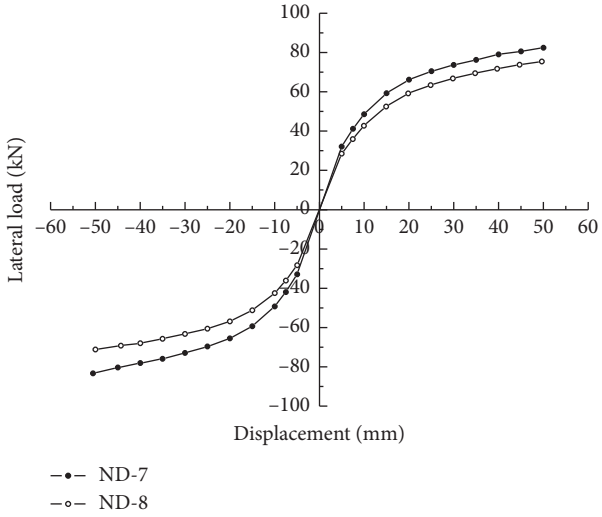

Figure 32: Skeleton curves of slit width 30 mm.

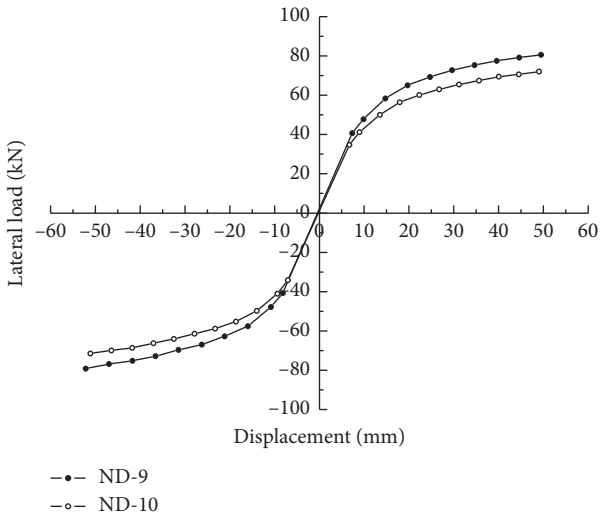

Figure 33: Skeleton curves of slit width 40 mm.

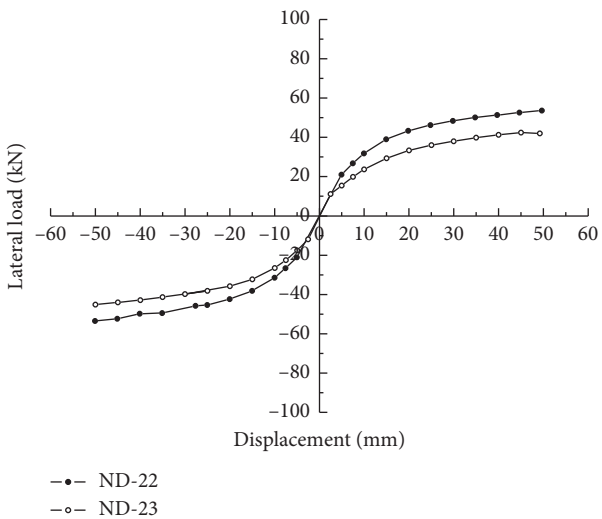

Figure 34: Skeleton curves of slit width 300 mm.

Table 11: Loads, displacement and ductility of different boundary conditions.

Specimen	Slit width (mm)	Boundary conditions	Yield load (kN)	Δ_y (mm)	Ultimate load (kN)	Δ_u (mm)	Ductility
ND5	20	UZ	62.39	13.58	89.86	49.48	3.64
ND6	20	—	56.82	13.64	78.87	48.83	3.58
ND7	30	UZ	53.61	13.87	82.44	50.05	3.61
ND8	30	—	51.76	13.98	75.45	49.63	3.55
ND9	40	UZ	57.93	14.09	80.60	49.47	3.51
ND10	40	—	51.59	14.05	72.02	49.04	3.49
ND22	300	UZ	39.24	15.41	53.65	49.62	3.22
ND23	300	—	29.47	15.73	42.01	49.24	3.13

Δ_y: Yield displacement; Δ_u: Ultimate load.

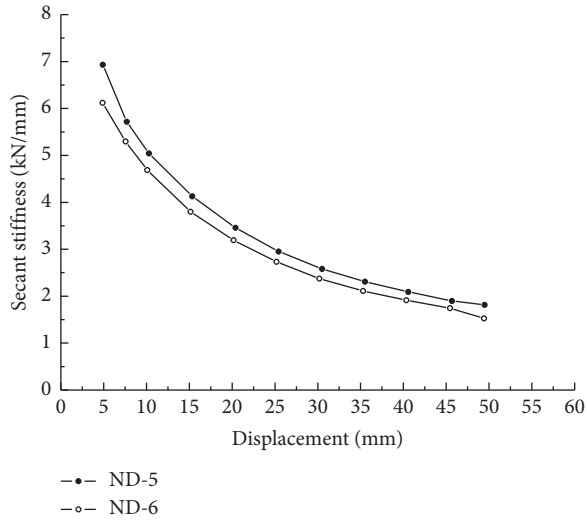

Figure 35: Stiffness curves of slit width 20 mm.

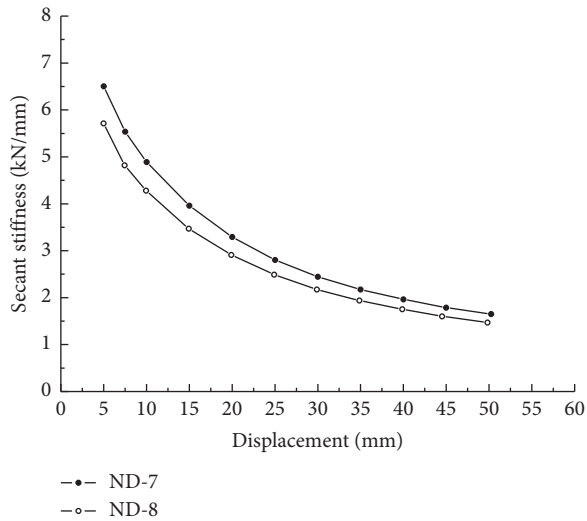

Figure 36: Stiffness curves of slit width 30 mm.

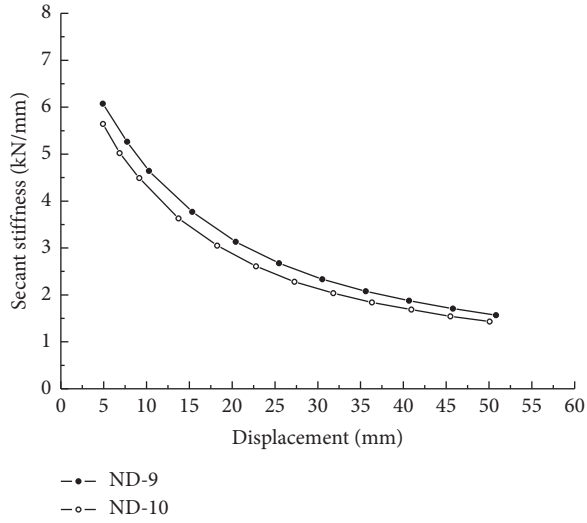

Figure 37: Stiffness curves of slit width 40 mm.

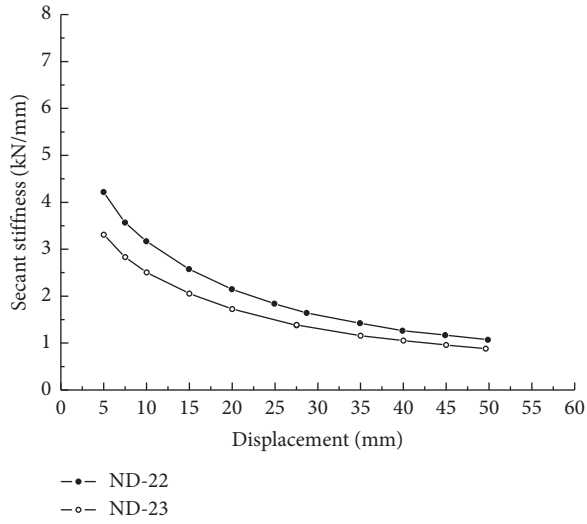

Figure 38: Stiffness curves of slit width 300 mm.

Table 12: Stiffness of different boundary conditions.

Specimen	Slit width (mm)	Thickness (mm)	Initial stiffness (kN/mm)	Ultimate stiffness (kN/mm)
ND5	20	UZ	6.93	1.82
ND6	20	—	6.12	1.53
ND7	30	UZ	6.51	1.65
ND8	30	—	5.72	1.47
ND9	40	UZ	6.08	1.57
ND10	40	—	5.64	1.43
ND22	300	UZ	4.22	1.07
ND23	300	—	3.31	0.88

6. Conclusions

Two specimens, Specimen ND-1 and Specimen ND-2, are compared. There were 24 models to research the seismic behavior on different influence parameters. The parameters are slit width, thickness of corrugated steel plate shear walls, concrete strength of nonductile RC frame, and boundary conditions of corrugated steel plate shear walls at slotted

parts. Hysteresis curves, skeleton curves, ductility, and stiffness curves were researched in the paper. The following conclusions can be drawn:

(i) To verify the availability of the models, the simulated results were compared with experimental results. The effective model indicated that the corrugated steel plate shear walls slotted with columns played a positive role in seismic behavior.

(ii) The paper selected four slit widths (10 mm, 100 mm, 200 mm, and 400 mm) to study the seismic performance of reinforced nonductile RC frame. Hysteresis curves and skeleton curves manifested that the strength was declined when the slit width was larger. Ductility had been improved in the strengthening with corrugated steel plate shear walls. Ductility was above 3.0 and the ductility was larger with the slit width being smaller. Stiffness was enhanced with the decrease of slit width.

(iii) With the thickness of corrugated steel plate shear walls increasing, the strength, ductility, stiffness, and energy dissipating capacity were enhanced greatly. The reinforced nonductile RC frame had enough seismic performance.

(iv) With concrete strength increasing, the strength and stiffness were enhanced gradually. The influence of concrete strength on ductility was little.

(v) Boundary conditions of corrugated steel plate shear walls at slotted parts were an important influence on nonductile RC frame. With the boundary conditions, larger strength, ductility, and stiffness can be gained. However, the increase was not very significant.

(vi) When the slit width was within the scope of 300 mm, the seismic behavior of nonductile RC frame slotted with corrugated steel plate shear walls could gain good performance.

Data Availability

All relevant data used in this study are within the paper and its Optional Supplementary Materials.

Conflicts of Interest

The authors declare that they have no conflicts of interest.

Acknowledgments

The authors would like to acknowledge the Natural Science Foundation of the Jiangsu Higher Education Institutions of China (No. 18KJB560002), the Research Project of Ministry of Housing and Urban-Rural Development of Jiangsu province (No. 2017ZD233), Research Project of Changzhou Institute of Technology (No. YN1722), the Project of Changzhou Science and Technology Program (No. CE20195034), the Project of Undergraduate Training Program for Innovation and Entrepreneurship (Nos. 2019064Z and 202011055051Y), and the Research Project of Changzhou Institute of Technology (No. YN20019).

References

[1] P. Z. Zhang and J. P. Ou, "Seismic performance analysis and evaluation for low-ductile RC frame structures," *Journal of Building Structures*, vol. 34, no. 12, pp. 11–18, 2013, in Chinese.

[2] K. J. Elwood, "Modelling failures in existing reinforced concrete columns," *Canadian Journal of Civil Engineering*, vol. 31, no. 5, pp. 846–859, 2004.

[3] S. Yavari, K. J. Elwood, and C.-l. Wu, "Collapse of a nonductile concrete frame: evaluation of analytical models," *Earthquake Engineering and Structural Dynamics*, vol. 38, no. 2, pp. 225–241, 2009.

[4] C.-l. Wu, W.-W. Kuo, Y.-S. Yang et al., "Collapse of a nonductile concrete frame: shaking table tests," *Earthquake Engineering and Structural Dynamics*, vol. 38, no. 2, pp. 205–224, 2009.

[5] C. D. Comartin, T. Anagnos, H. Faison, M. Greene, and J. Moehle, "The concrete coalition: building a network to address nonductile concrete buildings," in *Proceedings of the 14th World Conference On Earthquake Engineering: Innovation Practice Safety*, International Association for Earthquake Engineering, Beijing, China, October 2008.

[6] M. B. Shoraka, *Collapse assessment of non-ductile reinforced concrete moment frames*, Ph.D. Dissertation, Department of Civil Engineering, University of British Columbia, Vancouver, BC, Canada, 2012.

[7] H. Aslani and E. Miranda, "Fragility assessment of slab-column connections in existing non-ductile reinforced concrete buildings," *Journal of Earthquake Engineering*, vol. 9, no. 6, pp. 755–775, 2005.

[8] E. F. Deng, L. Zong, and Y. Ding, "Numerical and analytical study on initial stiffness of corrugated steel plate shear walls in modular construction," *Steel and Composite Structures*, vol. 32, no. 3, pp. 347–359, 2019.

[9] M. Shariati, "Numerical study on the structural performance of corrugated low yield point steel plate shear walls with circular openings," *Steel and Composite Structures*, vol. 33, no. 4, pp. 569–581, 2019.

[10] W. J. Wu, W. X. Song, and S. F. Jiang, "Multi-scale modeling and seismic performance analysis on non-ductile frame structures," *Journal of Basic Science and Engineering*, vol. 26, no. 6, pp. 164–174, 2018, in Chinese.

[11] W. Sae-Long, S. Limkatanyu, and W. Prachasaree, "Nonlinear frame element with shear- flexure interaction for seismic analysis of non-ductile reinforced concrete columns," *International Journal of Concrete Structures and Materials*, vol. 13, no. 1, pp. 13–32, 2019.

[12] M. B. Shoraka, T. Y. Yang, and K. J. Elwood, "Seismic loss estimation of non-ductile reinforced concrete buildings," *Earthquake Engineering and Structural Dynamics*, vol. 42, no. 2, pp. 297–310, 2013.

[13] L. L. Song and M. Ezechia, "Study on seismic performance of non-ductile RC frames retrofitted by SMA braces," *Building Structure*, vol. 48, no. S2, pp. 761–764, 2018, in Chinese.

[14] A. Khampanit, S. Leelataviwat, J. Kochanin, and P. Warnitchai, "Energy-based seismic strengthening design of non-ductile reinforced concrete frames using buckling-restrained braces," *Engineering Structures*, vol. 81, no. 1, pp. 110–122, 2014.

[15] L. D. Sarno and G. Manfredi, "Seismic retrofitting with buckling restrained braces: application to an existing non-

ductile RC framed building," *Soil Dynamicsand Earthquake Engineering*, vol. 30, no. 11, pp. 1279–1297, 2010.
[16] W. H. Chen, Z. H. Qiao, and W. R. Shou, "Experimental study on seismic performance of CFRP-retrofitted earthquake damaged non-ductile RC frames," *Journal of Southwest Jiaotong University*, vol. 1, no. 5, pp. 1–8, 2019, in Chinese.
[17] D. G. Lv, X. H. Yu, and N. Li, "Seismic collapse fragility analysis for non-ductile RC frame structures retrofitted with FRP," *Journal of Building Structures*, vol. 36, no. S2, pp. 112–118, 2015, in Chinese.
[18] F. W. Qiu and P. Pan, "Quasi-static loading and control for structural test," *Chinese Journal of Civil Engineering*, vol. 35, no. 1, pp. 1–10, 2002, in Chinese.
[19] N. Feng, C. Wu, and P. Cao, "Seismic performance of infilled RC frames with steel corrugated shear walls," *Magazine of Concrete Research*, vol. 72, no. 11, pp. 541–551, 2020.
[20] Q. H. Zhao, J. Qiu, B. C. Hao et al., "Lateral behavior of vertically-corrugated steel plate shear walls connected with beams only," *Journal of Tianjin University(Science and Technology)*, vol. 52, no. S2, pp. 46–53, 2019.
[21] N. Feng, P. Cao, K. Wu, and P. Zhang, "Experimental investigation on strengthening of infilled frame structures by profiled steel sheet shear walls," *Advances in Structural Engineering*, vol. 19, no. 4, pp. 703–714, 2016.
[22] Design code, *AISC Steel Design Guide 20: Steel Plate Shear Walls*, AISC, Chicago, IL, USA, 2006.